Indoor Pedestrian Navigation using an INS/EKF framework for Yaw Drift Reduction and a Foot-mounted IMU

A.R. Jiménez, F. Seco, J.C. Prieto and J. Guevara
Consejo Superior de Investigaciones Científicas.
Ctra. Campo Real km. 0.2; La Poveda, 28500, Arganda del Rey.
Madrid (Spain).
Telephone: (34) 918711900, Fax: (34) 918717050
Email: arjimenez@iai.csic.es
Web: http://www.iai.csic.es/lopsi

***Abstract*—The estimation of the position of a person in a building is a must for creating Intelligent Spaces. State-of-the-art Local Positioning Systems (LPS) require a complex sensor-network infrastructure to locate with enough accuracy and coverage. Alternatively, Inertial Measuring Units (IMU) can be used to estimate the movement of a person; a methodology that is called Pedestrian Dead-Reckoning (PDR). In this paper, we describe and implement a Kalman-based framework, called INS-EKF-ZUPT (IEZ), to estimate the position and attitude of a person while walking. IEZ makes use of an Extended Kalman filter (EKF), an INS mechanization algorithm, a Zero Velocity Update (ZUPT) methodology, as well as, a stance detection algorithm. As the IEZ methodology is not able to estimate the heading and its drift (non-observable variables), then several methods are used for heading drift reduction: ZARU, HDR and Compass. The main contribution of the paper is the integration of the heading drift reduction algorithms into a Kalman-based IEZ platform, which represents an extended PDR methodology (IEZ+) valid for operation in indoor spaces with local magnetic disturbances. The IEZ+ PDR methodology was tested in several simulated and real indoor scenarios with a low-performance IMU mounted on the foot. The positioning errors were about 1% of the total travelled distance, which are good figures if compared with other works using IMUs of higher performance.**

I. Introduction

In order to fulfil the *Intelligent Spaces*' goals, further research in artificial intelligence and sensor network technology, is required. One important topic is the accurate and continuous location of persons indoors. Local Positioning Systems (LPS) are being investigated, using ultrasound, radio or vision technology [1], but in some cases beacon-free solutions are preferable since they do not depend on a pre-installed infrastructure.

During the last decade several beacon-free methodologies have been proposed for accurate person's position estimation based on inertial sensors [2]-[14]. These methodologies, often called Pedestrian Dead-Reckoning (PDR) solutions, integrate step lengths and orientation estimations at each detected step, so as to compute the absolute position and orientation of a person. Some PDR approaches assume a smooth walk on horizontal surfaces, and others are valid for uneven terrain with complicated gait patterns. PDR has been proposed for a large range of applications, such as defense, emergency rescue workers, smart offices, and so on. PDR positioning accuracy, normally ranges from 0.3% to 10% of the total travelled distance, but this figures strongly depend on the algorithm implemented and the particular inertial sensor technology employed.

Inertial Measurement Units (IMU), normally contain several accelerometers, gyroscopes, magnetometers and even pressure sensors. The IMU sensors in aerospace applications, based on gimballed sensors or laser based gyroscopes, are bulky but provide a very accurate estimation with a low drift [9]. The size and performance of an inertial sensor are linearly dependent parameters, so the smaller the sensor the lower performance is expected. Low- size and weight units such as those based on Micro-Electro-Mechanical (MEMS) sensors are becoming very popular, but they have a significant bias and therefore suffer large drifts after integration.

In this paper, we describe and implement a Kalman-based framework (IEZ), following the Foxlin work [14], to estimate the position and attitude of a person while walking (section II). Several methods for heading Drift reduction: ZARU, HDR and Compass, have been implemented and integrated into the Kalman-based IEZ framework (section III). Finally, these extended PDR algorithms (IEZ+) were tested in several simulated and real indoor scenarios with an IMU mounted on the foot (section IV).

II. The Kalman-based Inertial PDR method

The method for Pedestrian Dead-Reckoning (PDR) has been implemented in a Kalman-based framework using the guidelines of Foxlin [14]. The idea is to use an Extended Kalman Filter (EKF) to estimate the errors of an Inertial Navigation System (INS), which accumulate due to the IMU sensor biases. The EKF is updated with velocity measurements by the Zero-Velocity-Update strategy (ZUPT) every time the foot is on the floor. We call this Kalman-based framework

978-1-4244-7157-7/10/$26.00 ©2010 IEEE

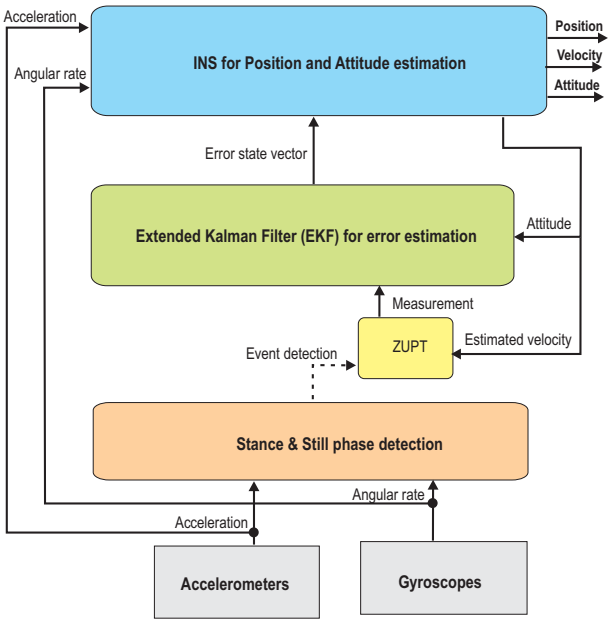

Fig. 1. The IEZ Kalman-based framework used for pedestrian dead-reckoning. It has four main blocks: 1) an INS mechanization algorithm adapted to incorporate the error estimations from an EKF, 2) a Extended Kalman Filter (EKF) that estimates the errors states related to the INS, 3) a Zero-Velocity-Update (ZUPT) block that feeds the EKF with the measured errors in velocity, and 4) a Stance&Still detection algorithm to determine when the person is at rest (Still) or with the foot on the ground while walking (Stance). In this framework 3 accelerometers and 3 gyroscopes are used in an IMU mounted on the foot of a person.

INS-EKF-ZUPT, or just IEZ, for short. Figure 1 shows the main blocks in the IEZ PDR methodology.

A. Inertial Navigation (INS)

The INS algorithm uses the accelerometer and gyroscopic readings, in the sensor body (b) frame of reference, ($\mathbf{a}_k^b$ and $\boldsymbol{\omega}_k^b$, respectively) which are taken at every sample interval Δt at discrete sampling times k. A classical INS mechanization was implemented, including some modifications to cope with the information provided by the EKF throughout the error state vector: $\delta\mathbf{x}_k = [\delta\boldsymbol{\varphi}_k, \delta\boldsymbol{\omega}_k^b, \delta\mathbf{r}_k, \delta\mathbf{v}_k, \delta\mathbf{a}_k^b]$. This 15-element vector contains the estimated biases for accelerometers and gyroscopes ($\delta\boldsymbol{\omega}^b$ and $\delta\mathbf{a}^b$, respectively), as well as, the errors in attitude ($\delta\boldsymbol{\varphi}$) and the errors in position and velocity ($\delta\mathbf{r}, \delta\mathbf{v}$). All these 5 components have 3 elements each, corresponding to a three-dimensional estimation. Details of the designed INS block for use in the IEZ framework are shown in Fig. 2 and explained in the following.

This INS mechanization process has five main phases:

1) Bias compensation of raw acceleration and gyroscopic values based on Kalman bias estimates (1.a & 1.b in Fig. 2).
2) Integration of gyroscopic values in order to estimate the attitude (2).
3) Remove the gravitational component in acceleration readings (3).
4) Integration of acceleration values to estimate the velocity and, after a second integration, the position (4.a & 4.b).
5) Refinement of position, velocity and attitude based on Kalman error estimates (5.a, 5.b & 5.c).

The first phase for bias compensation consists in subtracting to the raw acceleration and gyroscopic sensor data ($\boldsymbol{\omega}_k^b$ and $\mathbf{a}_k^b$ respectively), the bias terms estimated by the Kalman filter (positions 4-6 and 13-15 in the error state vector for gyro and accelerometers biases, respectively):

$$\begin{cases} \boldsymbol{\omega}_k^{'b} &= \boldsymbol{\omega}_k^b - \delta\mathbf{x}_{k-1}(4:6) &= \boldsymbol{\omega}_k^b - \delta\boldsymbol{\omega}_{k-1}^b \\ \mathbf{a}_k^{'b} &= \mathbf{a}_k^b - \delta\mathbf{x}_{k-1}(13:15) &= \mathbf{a}_k^b - \delta\mathbf{a}_{k-1}^b \end{cases}, \quad (1)$$

where $\boldsymbol{\omega}_k^{'b}$ and $\mathbf{a}_k^{'b}$ denote the bias-compensated gyroscopic and acceleration sensor readings, respectively.

In the second phase, we update the sensor orientation, with respect to the navigation frame (n, defined to be Noth-West-Up on the ground), based on the bias-compensated gyroscopic readings. A *Padé* approximation of the exponential function is used for this orientation update [11]:

$$\mathbf{C}_{b_{k|k-1}}^n = f(\mathbf{C}_{b_{k-1|k-1}}^n, \boldsymbol{\omega}_k^{'b}) = \mathbf{C}_{b_{k-1|k-1}}^n \cdot \frac{2\mathbf{I}_{3\times3} + \delta\boldsymbol{\Omega}_k \cdot \Delta t}{2\mathbf{I}_{3\times3} - \delta\boldsymbol{\Omega}_k \cdot \Delta t}, \quad (2)$$

where $\mathbf{C}_{b_{k|k-1}}^n$ is the rotation matrix that transforms from the body (b) to the navigation (n) frame, which is updated with the gyroscopic information at time k but not yet corrected by the EKF; $\mathbf{C}_{b_{k-1|k-1}}^n$ is the last rotation matrix available that was already corrected by the EKF after the filter update at time $k-1$; and $\delta\boldsymbol{\Omega}_k$ is the skew symmetric matrix for angular rates used to define the small angular increments in orientation:

$$\delta\boldsymbol{\Omega}_k = \begin{bmatrix} 0 & -\boldsymbol{\omega}_k^{'b}(3) & \boldsymbol{\omega}_k^{'b}(2) \\ \boldsymbol{\omega}_k^{'b}(3) & 0 & -\boldsymbol{\omega}_k^{'b}(1) \\ -\boldsymbol{\omega}_k^{'b}(2) & \boldsymbol{\omega}_k^{'b}(1) & 0 \end{bmatrix}. \quad (3)$$

Note that the rotation matrix $\mathbf{C}_{b_{k-1|k-1}}^n$ is post-multiplied by the term that represents the small change in orientation, since this rotation is with respect to the sensor body reference frame (b).

In the third phase, the acceleration of gravity is removed from the sensor readings. Initially, the accelerations, $\mathbf{a}_k^{'b}$, are transformed from the sensor body coordinate frame (b) to the navigation frame (n), and then the value of g (9.8 m/s) is subtracted to the "vertical" component of acceleration:

$$\breve{\mathbf{a}}_k = \mathbf{C}_{b_{k|k-1}}^n \cdot \mathbf{a}_k^{'b} - [0, 0, g]. \quad (4)$$

In the fourth phase, the gravity-free acceleration value $\breve{\mathbf{a}}_k$, is integrated to obtain the velocity in the navigation frame, $\mathbf{v}_{k|k-1}$, prior to the EKF correction at time k:

$$\mathbf{v}_{k|k-1} = \mathbf{v}_{k-1|k-1} + \breve{\mathbf{a}}_k \cdot \Delta t. \quad (5)$$

This velocity is integrated to obtain the sensor position in the navigation frame:

$$\mathbf{r}_{k|k-1} = \mathbf{r}_{k-1|k-1} + \mathbf{v}_{k|k-1} \cdot \Delta t. \quad (6)$$

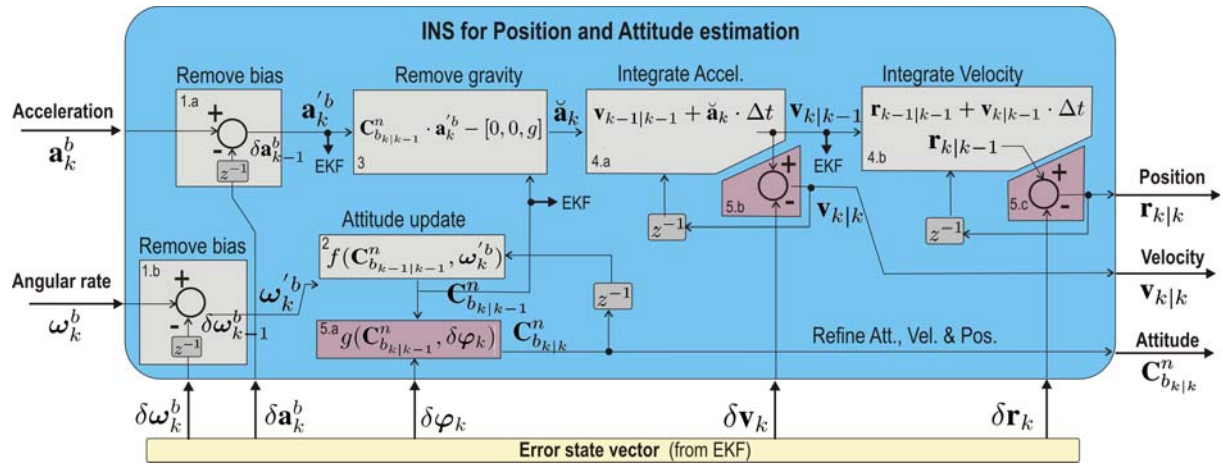

Fig. 2. Details of the INS mechanization algorithm adapted to be used in cooperation with the EKF in the IEZ framework. It accepts the estimated sensor biases for accelerometers and gyroscopes ($\delta\boldsymbol{\omega}^b$ and $\delta\mathbf{a}^b$, respectively), as well as, the errors in attitude ($\delta\boldsymbol{\varphi}$) and the errors in velocity and position ($\delta\mathbf{r}, \delta\mathbf{v}$).

Finally, in the fifth phase, we correct the previously computed position and velocity estimates once the EKF has been updated with the measurements at time k, by making use of the filtered Kalman error state $\delta\mathbf{x}_k$:

$$\begin{cases} \mathbf{r}_{k|k} = \mathbf{r}_{k|k-1} - \delta\mathbf{x}_k(7:9) = \mathbf{r}_{k|k-1} - \delta\mathbf{r}_k \\ \mathbf{v}_{k|k} = \mathbf{v}_{k|k-1} - \delta\mathbf{x}_k(10:12) = \mathbf{v}_{k|k-1} - \delta\mathbf{v}_k \end{cases}. \tag{7}$$

The attitude refinement is achieved by updating the rotation matrix, $\mathbf{C}^n_{b_{k|k-1}}$, with the three angle errors estimated by the EKF for roll, pitch and yaw ($\delta\boldsymbol{\varphi}_k$). Assuming that those angle errors are small, the corrected rotation matrix, $\mathbf{C}^n_{b_{k|k}}$, is computed, using another *Padé* approximation, as:

$$\mathbf{C}^n_{b_{k|k}} = g(\mathbf{C}^n_{b_{k|k-1}}, \delta\boldsymbol{\varphi}_k) = \frac{2\mathbf{I}_{3\times3} + \delta\boldsymbol{\Theta}_k}{2\mathbf{I}_{3\times3} - \delta\boldsymbol{\Theta}_k} \cdot \mathbf{C}^n_{b_{k|k-1}} \tag{8}$$

where $\delta\boldsymbol{\Theta}_k$ is the skew symmetric matrix for small angles

$$\delta\boldsymbol{\Theta}_k = -\begin{bmatrix} 0 & -\delta\boldsymbol{\varphi}_k(3) & \delta\boldsymbol{\varphi}_k(2) \\ \delta\boldsymbol{\varphi}_k(3) & 0 & -\delta\boldsymbol{\varphi}_k(1) \\ -\delta\boldsymbol{\varphi}_k(2) & \delta\boldsymbol{\varphi}_k(1) & 0 \end{bmatrix}. \tag{9}$$

Note that the original rotation matrix has been premultiplied by the incremental rotation term since this small change in orientation is with respect to the navigation frame (n).

B. The Extended Kalman filter (EKF)

The PDR navigation state transition model is a non-linear function of the states, but it can be linearized around a state estimate [14], [11]. If the 15-element error state vector at time k is

$$\delta\mathbf{x}_{k|k} = \delta\mathbf{x}_k = [\delta\boldsymbol{\varphi}_k, \delta\boldsymbol{\omega}^b_k, \delta\mathbf{r}_k, \delta\mathbf{v}_k, \delta\mathbf{a}^b_k], \tag{10}$$

then, the linearized state transition model is:

$$\delta\mathbf{x}_{k|k-1} = \boldsymbol{\Phi}_k\delta\mathbf{x}_{k-1|k-1} + \mathbf{w}_{k-1}, \tag{11}$$

where $\delta\mathbf{x}_{k|k-1}$ is the predicted error state, $\delta\mathbf{x}_{k-1|k-1}$ is the last filtered error state at time $k-1$, $\mathbf{w}_{k-1}$ is the process noise with covariance matrix $\mathbf{Q}_k = E(\mathbf{w}_k\mathbf{w}_k^T)$, and $\boldsymbol{\Phi}_k$ is the 15×15 state transition matrix:

$$\boldsymbol{\Phi}_k = \begin{bmatrix} \mathbf{I} & \Delta t\cdot\mathbf{C}^n_{b_{k|k-1}} & 0 & 0 & 0 \\ 0 & \mathbf{I} & 0 & 0 & 0 \\ 0 & 0 & \mathbf{I} & \Delta t\cdot\mathbf{I} & 0 \\ -\Delta t\cdot\mathbf{S}(\mathbf{a}^{'n}_k) & 0 & 0 & \mathbf{I} & \Delta t\cdot\mathbf{C}^n_{b_{k|k-1}} \\ 0 & 0 & 0 & 0 & \mathbf{I} \end{bmatrix}. \tag{12}$$

The term $\mathbf{S}(\mathbf{a}^{'n}_k)$ in matrix $\boldsymbol{\Phi}_k$ is the skew symmetric matrix for accelerations that allows the EKF to act as an inclinometer, estimating the pitch and roll of the sensor:

$$\mathbf{S}(\mathbf{a}^{'n}_k) = \begin{bmatrix} 0 & -a_{z_k} & a_{y_k} \\ a_{z_k} & 0 & -a_{x_k} \\ -a_{y_k} & a_{x_k} & 0 \end{bmatrix}. \tag{13}$$

$\mathbf{a}^{'n}_k$ is the bias-corrected acceleration that has been transformed to the navigation frame of reference:

$$\mathbf{a}^{'n}_k = \mathbf{C}^n_{b_{k|k-1}} \cdot \mathbf{a}^{'b}_k = (a_{x_k}, a_{y_k}, a_{z_k}). \tag{14}$$

The measurement model is

$$\mathbf{z}_k = \mathbf{H}\delta\mathbf{x}_{k|k} + \mathbf{n}_k \tag{15}$$

where $\mathbf{z}_k$ is the error measurements, $\mathbf{H}$ is the measurement matrix, and $\mathbf{n}_k$ is the measurement noise with covariance matrix $\mathbf{R}_k = E(\mathbf{n}_k\mathbf{n}_k^T)$.

The filtered error state $\delta\mathbf{x}_{k|k}$ at time k is obtained after a measurement at time k is available, with the Kalman update equation:

$$\delta\mathbf{x}_{k|k} = \delta\mathbf{x}_{k|k-1} + \mathbf{K}_k\cdot[\mathbf{m}_k - \mathbf{H}\delta\mathbf{x}_{k|k-1}], \tag{16}$$

where $\mathbf{K}_k$ is the Kalman gain, $\mathbf{m}_k$ is the actual error measurement, and $\delta\mathbf{x}_{k|k-1}$ is the predicted error state.

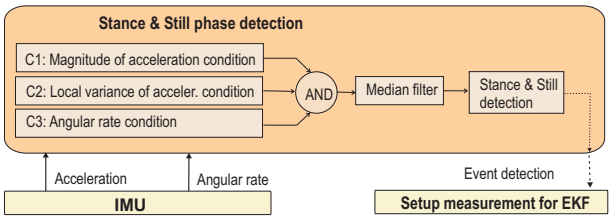

Fig. 3. *Stance* and *Still* detection block used in the IEZ framework.

The Kalman gain is calculated with the usual formula:

$$\mathbf{K}_k = \mathbf{P}_{k|k-1}\mathbf{H}^T(\mathbf{H}\mathbf{P}_{k|k-1}\mathbf{H}^T + \mathbf{R}_k)^{-1}. \quad (17)$$

where $\mathbf{P}_{k|k-1}$ is the estimation error covariance matrix, that is computed at time k based on measurements received at time k-1, with the classical form: $\mathbf{P}_{k|k-1} = \mathbf{\Phi}_{k-1}\mathbf{P}_{k-1|k-1}\mathbf{\Phi}_{k-1}^T + \mathbf{Q}_{k-1}$. The covariance matrix $\mathbf{P}_{k|k}$ at time k is then computed using the Kalman gain in the Joseph form equation: $\mathbf{P}_{k|k} = (\mathbf{I}_{15\times15} - \mathbf{K}_k\mathbf{H})\mathbf{P}_{k|k-1}(\mathbf{I}_{15\times15} - \mathbf{K}_k\mathbf{H})^T + \mathbf{R}_k$.

It is important to mention that the non-bias error terms of the filtered state vector, $\delta\mathbf{x}_{k|k}$, are reset to zero after the INS uses them to refine the current attitude, velocity and position. This is because those errors are already compensated and incorporated into the INS estimations. The only terms that are maintained over time in the EKF filter are the gyro and accelerometer biases, i.e. $\delta\boldsymbol{\omega}_k^b$ and $\delta\mathbf{a}_k^b$.

The actual error measurement $\mathbf{m}_k$ that feeds the EKF, is calculated for ZUPT as: $\mathbf{m}_k = \mathbf{v}_{k|k-1} - [0,0,0]$, where the zero vector means that at stance we know that the velocity of the foot is almost zero. The measurement matrix, $\mathbf{H}$, for ZUPT update is a 3 by 15 matrix like this: $\mathbf{H} = [\mathbf{0}_{3\times3}, \mathbf{0}_{3\times3}, \mathbf{0}_{3\times3}, \mathbf{I}_{3\times3}, \mathbf{0}_{3\times3}]$. It selects the velocity error components from the error state matrix $\delta\mathbf{x}_k$, i.e. the 10th to 12th terms.

C. Stance detection

The EKF gets feedback from measurements, only when the person's foot is detected to be stationary on the ground (totally still, or in a stance phase during walk). Most algorithms in the literature for stance detection rely on basic signal processing techniques with accelerometers [5], [13] or gyroscopes [2]. They properly work in many situations but occasionally fail in slow and random walk [13]. We implement a multi-condition algorithm, that complements the implementation of [10] by using both sources of information (accelerometers and gyroscopes) and an order filter so as to make the detection process robust enough (see Fig. 3).

The three conditions ($C1$, $C2$ and $C3$) to declare a foot as stationary are:

1) The magnitude of the acceleration, $|\mathbf{a}_k| = [\mathbf{a}_k^b(1)^2 + \mathbf{a}_k^b(2)^2 + \mathbf{a}_k^b(3)^2]^{0.5}$ must be between two thresholds ($\text{th}_{a_{min}} = 9$ and $\text{th}_{a_{max}} = 11$ m/s^2).

$$C1 = \begin{cases} 1 & \text{th}_{a_{min}} < |\mathbf{a}_k| < \text{th}_{a_{max}} \\ 0 & \text{otherwise} \end{cases}. \quad (18)$$

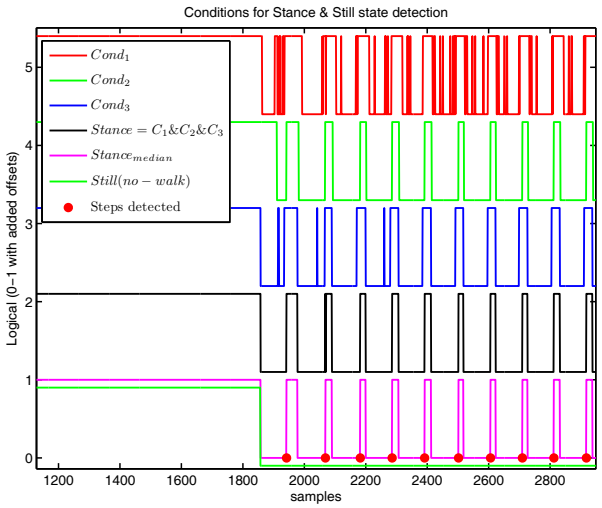

Fig. 4. Some results of the *Stance* and *Still* detection process.

2) The local acceleration variance, which highlights the foot activity, must be above a given threshold ($\text{th}_{\sigma_a} = 3$ m/s^2). The local variance is computed this way:

$$\sigma^2_{a_k^b} = \frac{1}{2s+1}\sum_{j=k-s}^{k+s}(a_k^b - \overline{a_k^b})^2, \quad (19)$$

where $\overline{a_k^b}$ is a local mean acceleration value, computed by this expression: $\overline{a_k^b} = \frac{1}{2s+1}\sum_{q=k-s}^{k+s} a_q$, and s defines the size of the averaging window ($s = 15$ samples). The second condition $C2$ is satisfied when:

$$C2 = \begin{cases} 1 & \sigma_{a_k^b} > \text{th}_{\sigma_a} \\ 0 & \text{otherwise} \end{cases}. \quad (20)$$

3) The magnitude of the gyroscope, $|\boldsymbol{\omega}_k| = [\boldsymbol{\omega}_k^b(1)^2 + \boldsymbol{\omega}_k^b(2)^2 + \boldsymbol{\omega}_k^b(3)^2]^{0.5}$, must be below a given threshold ($\text{th}_{\omega_{max}} = 50$ °/s).

$$C3 = \begin{cases} 1 & |\boldsymbol{\omega}_k| < \text{th}_{\omega_{max}} \\ 0 & \text{otherwise} \end{cases}. \quad (21)$$

The three logical conditions must be satisfied simultaneously for foot stationary detection, so a logical "AND" is applied, and the result is filtered out using a median filter with a neighboring window of 11 samples in total. The registered logical "1"s mark the *Stance* phase that occurs when the foot is stationary on the floor (while walking, or not). The *Still* phase, corresponding to a non-walking stationary foot, is detected from stance samples that are not surrounded by non-stance samples in a window larger than 2 seconds. Figure 4 shows results of this multi-condition stance detection process.

III. Methods to Reduce the Drift in Heading

The IEZ Kalman-based PDR method presented in last section (Fig. 1), accumulates large errors in orientation due to the bias in the gyroscopes. IEZ can not estimate it because the yaw orientation (ψ_k), and the gyroscopic bias ($\delta\boldsymbol{\omega}^b$) in the

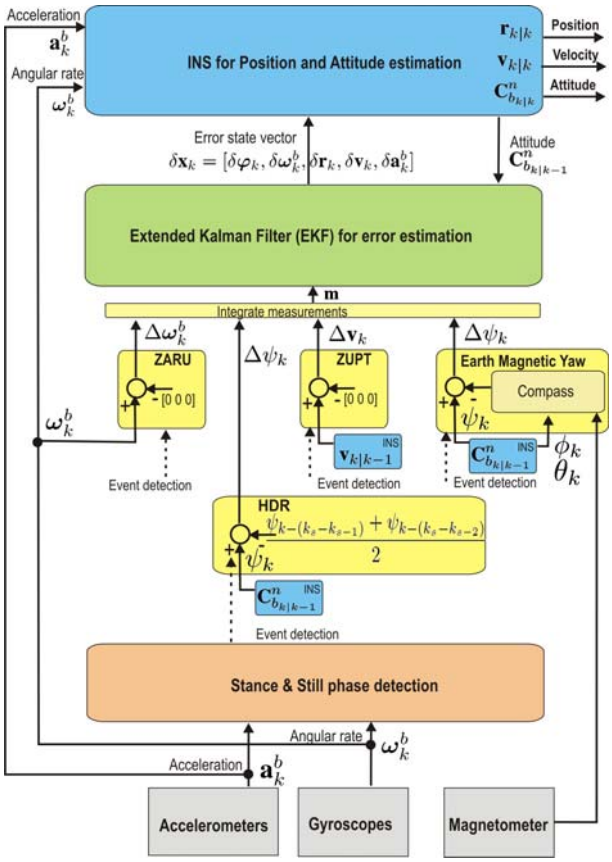

Fig. 5. The IEZ-extended PDR framework. It represents the same methodology as presented in Fig. 1 but adding the blocks for heading drift reduction: ZARU, HDR and Compass.

vertical axis, are not observable from ZUPT measurements alone [14]. Next subsections describe the integration in IEZ of some approaches to reduce the drift in heading: ZARU [10], HDR [12], and the use of magnetometers as a compass. We focus on methods to reduce the drift without using any external infrastructure such as GPS and LPS, nor map-matching techniques. See Fig. 5 to view how these methods are integrated in the IEZ framework.

A. Zero angular rate update (ZARU)

ZARU stands for Zero Angular Rate Update [10]. So, the idea is to feed the EKF with measurements of the measured error in the angular rate, while the foot is still.

$$\Delta\boldsymbol{\omega}_k^b = \boldsymbol{\omega}_k^b - [0,0,0]. \tag{22}$$

If ZARU is integrated in the IEZ framework, then its measurement matrix must be:

$$\mathbf{H} = \begin{bmatrix} \mathbf{0}_{3\times3} & \mathbf{I}_{3\times3} & \mathbf{0}_{3\times3} & \mathbf{0}_{3\times3} & \mathbf{0}_{3\times3} \\ \mathbf{0}_{3\times3} & \mathbf{0}_{3\times3} & \mathbf{0}_{3\times3} & \mathbf{I}_{3\times3} & \mathbf{0}_{3\times3} \end{bmatrix}, \tag{23}$$

and the error measurement vector is the concatenation of the ZARU and ZUPT contributions:

$$\mathbf{m}_k = [\Delta\boldsymbol{\omega}_k^b, \Delta\mathbf{v}_k]. \tag{24}$$

B. Heuristic Heading Reduction (HDR)

HDR stands for Heuristic Heading Reduction. It was originally proposed by Borestein et al. [12]. It makes use of the fact that many corridors or paths are straight. So, the idea of the HDR algorithm is to detect when a person is walking straight, and in that case apply a correction to the gyro biases, in order to reduce the heading error.

In our paper we use the same hypothesis, but we implement it in a total different way as Borestein et al. did [12]. Instead of filtering the gyro signals with a binary I-controller, we work in the Yaw space, detecting a straight walk by analyzing the orientation change, $\Delta\psi_k$, among successive steps:

$$\Delta\psi_k = \psi_k - \frac{\psi_{k-(k_s-k_{s-1})} + \psi_{k-(k_s-k_{s-2})}}{2}, \tag{25}$$

where ψ_k is the heading of the foot at the current sample k computed as $\psi_k = \arctan(\mathbf{C}^n_{b_{k|k}}(2,1), \mathbf{C}^n_{b_{k|k}}(1,1))$; k_s is the sample of last detected step (red points in Fig. 4), and k_{s-1} is the sample of the previous to the last detected step. The right part of equation 25 takes the average of two Yaw values at positions within the previous stance phases that are correlative with the position of sample k in its own stance phase.

If the orientation change among successive steps, $\Delta\psi_k$, is small enough (below a given threshold), then it is assumed a straight-line walk; and the EKF is fed with some measurement, $\mathbf{m}_k$, to correct the heading error so as to make the trajectory straight:

$$\mathbf{m}_k = \begin{cases} \Delta\psi_k & |\Delta\psi_k| \leq \text{th}_{\Delta\psi} \\ 0 & \text{otherwise} \end{cases}, \tag{26}$$

If $|\Delta\psi_k|$ is larger than $\text{th}_{\Delta\psi}$, then the orientation change is considered to be a real variation in the trajectory of a person. In that case, no corrections are fed into the EKF. We use an angular value of 4 degrees as threshold $\text{th}_{\Delta\psi}$.

The measurement matrix, $\mathbf{H}$, when incorporating the ZUPT and HDR updates is a 4 by 15 matrix as follows:

$$\mathbf{H} = \begin{bmatrix} [001] & 0_{1\times3} & 0_{1\times3} & 0_{1\times3} & 0_{1\times3} \\ \mathbf{0}_{3\times3} & \mathbf{0}_{3\times3} & \mathbf{0}_{3\times3} & \mathbf{I}_{3\times3} & \mathbf{0}_{3\times3} \end{bmatrix}. \tag{27}$$

C. Electronic Compass

This drift compensation method is normally used in outdoor environments, where magnetic disturbances are moderate. Indoors, the magnetic disturbances can be severe and permanent for a given position of the user. Some authors [12] do not recommend the use of magnetometers indoors, but, conveniently treated, we believe they are very useful as an absolute reference for heading.

In order to use the magnetometer sensor as a compass, we first transform the sensor body readings into the navigation frame of reference, using the Roll (ϕ_k) and Pitch (θ_k) angles:

$$\mathbf{B}^n_k = \begin{bmatrix} \cos\theta_k & 0 & -\sin\theta_k \\ 0 & 1 & 0 \\ -\sin\theta_k & 0 & \cos\theta_k \end{bmatrix} \cdot \begin{bmatrix} 1 & 0 & 0 \\ 0 & \cos\phi_k & -\sin\phi_k \\ 0 & \sin\phi_k & \cos\phi_k \end{bmatrix} \cdot \mathbf{B}^b_k, \tag{28}$$

Fig. 6. Xsens IMU attached to the right foot using the shoe's laces.

where the roll and pitch angles are obtained from the rotation matrix, as follows: $\phi_k = \arctan(\mathbf{C}^n_{b_{k|k}}(3,2), \mathbf{C}^n_{b_{k|k}}(3,3))$ and $\theta_k = -\arcsin(\mathbf{C}^n_{b_{k|k}}(3,1))$.

After this transformation, the magnetic field components are geodetically levelled, so the heading angle (ψ_{compass_k}) is:

$$\psi_{\text{compass}_k} = -\arctan(\mathbf{B}^n_k(2)/\mathbf{B}^n_k(1)) - \text{M}_d \qquad (29)$$

where M_d is the earth magnetic declination at a given point on the earth surface.

The compass error measurement $\mathbf{m}_k$ for the EKF is

$$\mathbf{m}_k = \Delta\psi_k = \psi_k - \psi_{\text{compass}_k}. \qquad (30)$$

The measurement matrix, $\mathbf{H}$, for ZUPT and Compass estimation is equal to the HDR case (eq. 27).

D. The full integration of all methods in IEZ

Once defined each individual method for drift reduction (ZARU, HDR and Compass), the evaluation of all these methods merged into the same IEZ framework is quite straightforward. The measurement matrix would be a 7 by 15 matrix with these components:

$$\mathbf{H} = \begin{bmatrix} [001] & 0_{1\times3} & 0_{1\times3} & 0_{1\times3} & 0_{1\times3} \\ \mathbf{0}_{3\times3} & \mathbf{I}_{3\times3} & \mathbf{0}_{3\times3} & \mathbf{0}_{3\times3} & \mathbf{0}_{3\times3} \\ \mathbf{0}_{3\times3} & \mathbf{0}_{3\times3} & \mathbf{0}_{3\times3} & \mathbf{I}_{3\times3} & \mathbf{0}_{3\times3} \end{bmatrix}, \qquad (31)$$

and the measurement vector would be:

$$\mathbf{m}_k = [\Delta\psi_k, \Delta\boldsymbol{\omega}^b_k, \Delta\mathbf{v}_k]. \qquad (32)$$

IV. Tests

We have performed several tests in order to evaluate the performance of these PDR methods: IEZ, IEZ+ZARU, IEZ+HDR, IEZ+Compass and IEZ+ZARU+HDR+Compass. Some tests were performed by simulation, but most of them belong to real indoor scenarios, where the IMU is installed on the right foot of a person, as Fig. 6 shows.

	accelerometers	gyroscopes	magnetometers
Axes	3	3	3
Full Scale (FS)	$\pm$50 m/s^2	$\pm$300 deg/s	$\pm$750 mGauss
Linearity	0.2% of FS	0.1% of FS	0.2% of FS
Bias stability	0.02 m/s^2	1 deg/s	0.1 mGauss
Bandwidth	30 Hz	40 Hz	10 Hz
Max update rate	512 Hz	512 Hz	512 Hz

TABLE I
Performance of individual sensors in Xsens IMU

A. IMU description

We use a commercially available IMU, model MTi from Xsens Technologies B.V (Enschede, The Netherlands). Its size is 58x58x22 mm (WxLxH), and it weights 50 grams. It is configured to send data at 100 Hz.

The IMU has three orthogonally-oriented accelerometers, three gyroscopes and three magnetometers. The accelerometers and gyroscopes are MEMS solid state with capacitative readout, providing linear acceleration and rate of turn, respectively. Magnetometers use a thin-film magnetoresistive principle to measure the earth magnetic field.

The performance of each individual MEMS sensor within the MTi IMU are summarized in table I. They suffer from a significant bias, and this bias also varies over time, so PDR algorithms have the challenge of avoiding excessive error accumulation (drift) during integration.

B. EKF Tuning

The EKF in the IEZ and the extended IEZ+ frameworks had to be fine-tuned in order to obtain a stable operation, by selecting the values of matrixes $\mathbf{Q}_k$, $\mathbf{R}_k$ and $\mathbf{P}_{k|k-1}$.

The process noise covariance matrix, $\mathbf{Q}_k$, is initialized for $k = 1$ as a diagonal 15x15 matrix with these in-diagonal elements: $[1 \cdot 10^{-4}_{1\times3}$ rad$, 0_{1\times3}, 0_{1\times3}, 1 \cdot 10^{-4}_{1\times3}$ m/s$, 0_{1\times3}]$. The non-zero values correspond to the variance of gyroscopic and accelerometer sensors that is, in both cases, about $1 \cdot 10^{-4}$.

The measurement noise covariance matrix: $\mathbf{R}_k$ is a square matrix with rows and columns equal to the number, n, of measurements available (3 for ZUPT, 4 for IEZ+ZARU, 6 for IEZ+HDR, 7 for IEZ+ZARU+HDR, and so on). We set this matrix with in-diagonal elements with values of: 0.01 m/s for ZUPT, 0.1 rad/s for ZARU, and 0.1 rad HDR and Compass.

The state estimation covariance matrix, $\mathbf{P}_{k|k-1}$, is initialized as a diagonal 15x15 matrix with these in-diagonal elements: $[0_{1\times3}, 1 \cdot 10^{-2}_{1\times3}$ rad/s$, 0_{1\times3}, 0_{1\times3}, 1 \cdot 10^{-2}_{1\times3}$ m/s$^2]$.

The results of the PDR algorithms strongly depends on the selected values for these covariance matrixes, so the tuning must be done trying to find a consistent response among the state estimates and the state estimation covariance matrix.

C. Performance using simulated IMU data

We simulated the data an IMU would output when a person is walking along a pre-defined trajectory and the IMU is mounted on the foot. This simulator was useful to better tune the EKF, and also to add controlled noise and biases to any of the simulated sensors.

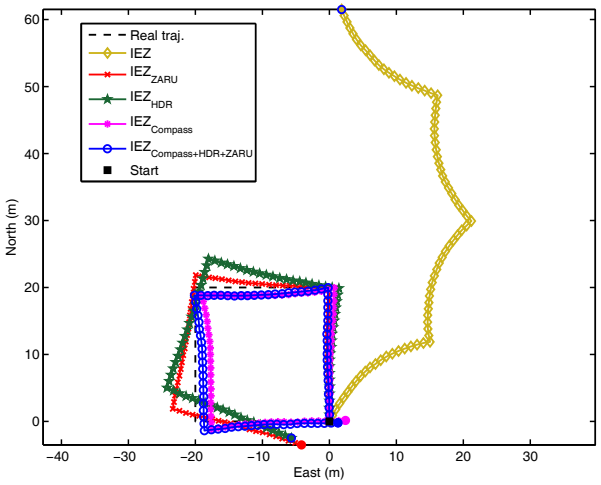

Fig. 7. Estimated trajectories from IEZ PDR algorithms, when using IMU simulated data.

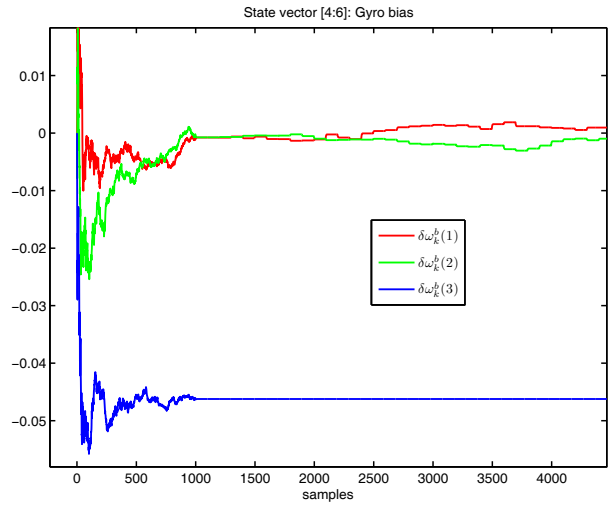

Fig. 8. Simulation of the evolution of the gyroscopic biases as estimated by the EKF in any of the IEZ+ extended methods. The vertical gyro bias converges in a few seconds to the true bias value (-0.05 rad/s).

A square trajectory of 20-meters-long side was simulated with a velocity of 1 m/s and a constant stride length of 1 meter. The gyroscopic biases were zero for X and Y axis, but was set to -0.05 rad/s in Z axis. Additionally, white Gaussian noise with zero mean was added to the accelerometer and gyroscopic samples ($\sigma_a = 0.01\ m/s^2$ and $\sigma_\omega = 0.01\ rad/s$). Figure 7 shows the positioning results using the IEZ and the different IEZ-extended algorithms. It is clear how a heading drift is accumulated due to the gyro bias using the IEZ method alone. However, we can see how the addition of several heading-related measurements to IEZ (ZARU+HDR+Compass) gives better results that in any other cases.

The estimation of the gyroscopic bias in the Z axis, using any of the IEZ+ extended methods, gets stable after 5 seconds (500 samples), as can be seen in Fig. 8. This initial period corresponds to the *Still* phase, just before the person starts to walk. Once the person is walking, the gyroscopic bias estimation is no longer changed since the state estimation covariance matrix converged to low values, which means that the bias estimation was reliably done.

D. Performance in real indoor environments

We tested the PDR algorithms in a real indoor environment. Tests were performed in building "A" of IAI-CSIC campus, both in a Counter-Clock-Wise (CCW) and Clock-Wise (CW) directions. Figures 9 and 10 show the estimated trajectories for a path 125 meters long, completed in 100 seconds.

It is important to mention that the Compass contribution is decisive in order to obtain accurate trajectories with respect the ideal path. This is valid even with several local magnetic perturbations that were detected along the path, as can be seen in Fig. 11.

As an initial performance index, we computed the positioning errors (difference between the initial and final position) with respect to the total travelled distance (TTD). The values presented in table II show the typical range of positioning errors found for several indoor tests like those presented in figures 9 and 10.

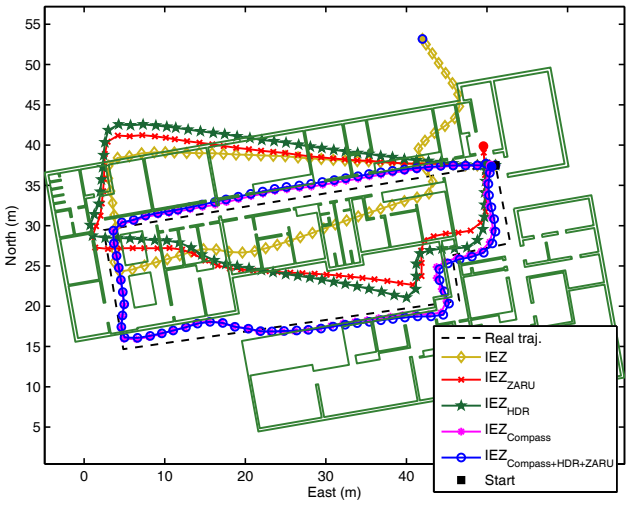

Fig. 9. Position estimation results using IEZ and several IEZ-extended PDR algorithms. The test is performed in building A of IAI-CSIC campus in a Counter-Clock-Wise (CCW) direction. The path is about 125 meters long, and it contains indoor as well as outdoor parts.

V. Conclusion

We have described, implemented and compared some of the most relevant Kalman-based PDR algorithms in the state of the art for pedestrian dead reckoning. The study consisted in the implementation of several methods for heading drift reduction, and the evaluation in a common IEZ PDR platform. We restricted the study to the use of an IMU sensor alone, i.e. without using any external infrastructure such as GPS, LPS or building-maps to correct the heading drift. The device was placed at the foot of the person because is the best position for accurate PDR.

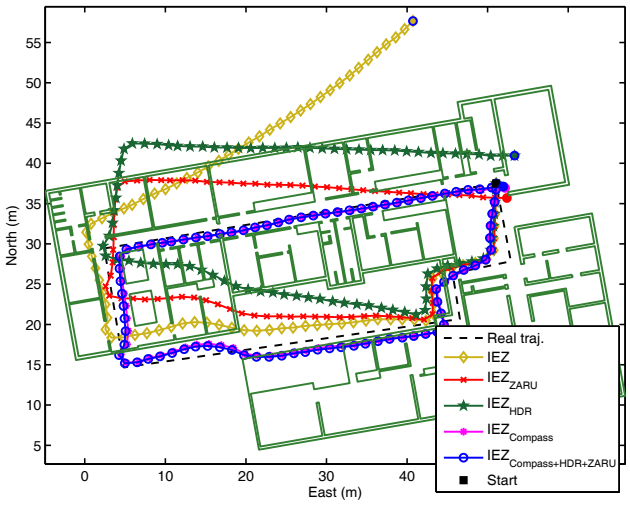

Fig. 10. The same test than in figure 9 but in Clock-Wise (CW) direction.

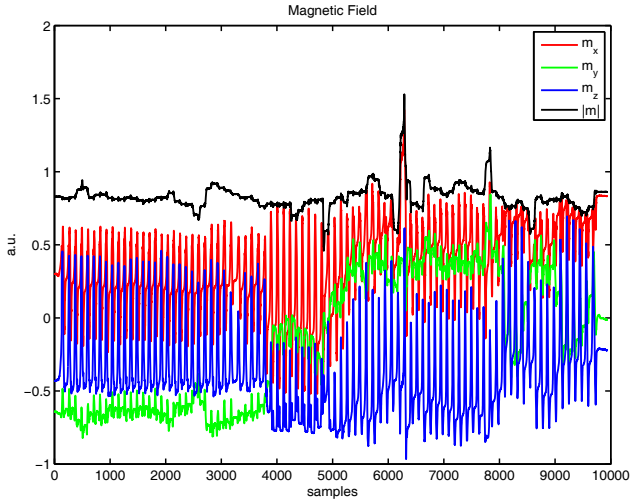

Fig. 11. Magnetometer readings, $\mathbf{B}_k^b$ (for k=1 to 10000), during the walking test in the indoor environment of Fig. 9. Note that the magnetic field magnitude is not constant along the path due to local magnetic disturbances.

PDR Method	Positioning errors (% of TTD)
IEZ	> 15
IEZ_{ZARU}	[4-8]
IEZ_{HDR}	[2-10]
$IEZ_{Compass}$	[0.6-5]
$IEZ_{ZARU+HDR+Compass}$	[0.3-1.5]

TABLE II
TYPICAL PERFORMANCE OF IEZ AND IEZ+ PDR ALGORITHMS FOR SEVERAL INDOOR TESTS. ERRORS IN PERCENTAGE OF TOTAL TRAVELLED DISTANCE (TTD).

The presented results shown that extended IEZ+ PDR algorithms can provide good solutions for estimating human trajectories, even in indoors environments with local magnetic disturbances, and even using a low-performance IMU. The uncorrected heading drift is proportional to the travelled distance but not to the time elapsed. The positioning error, for the IEZ+ method integrating ZARU+HDR+compass, is typically about 1% of the total travelled distance.

Future work will be focused to obtain a periodic absolute positioning update during the walk, in order to cancel out any drift. This update could be done with LPS sensors such as those based on RFID, WiFi, UWB or ultrasound; also matching PDR estimations with local maps; or using any kind of magnetic signatures that can be associated to a known position. Any of these approaches should provide a better indoor location of persons for *Intelligent Spaces* in scenarios such as homes, offices, healthcare spaces, emergencies, sport centers and so on.

ACKNOWLEDGMENT

The authors would like to thank the financial support provided by projects LEMUR (TIN2009-14114-C04-03), RESELAI (TIN2006-14896-C02-02) and LOCA (CSIC-PIE Ref.200450E430).

REFERENCES

[1] A.R. Jiménez, F. Seco, C. Prieto, and J. Roa, "Tecnologías sensoriales de localización para entornos inteligentes," in *I Congreso español de informática - Simposio de Computación Ubicua e Inteligencia Ambiental, UCAmI2005 (Granada)*, 2005, pp.75-86.

[2] R. Feliz, E. Zalama and J. Gómez, "Pedestrian tracking using inertial sensors," *Journal of Physical Agents*, vol. 3 (1), pp. 35-42, 2009.

[3] B. Beauregard, "Omnidirectional Pedestrian Navigation for First Responders," in *4th Workshop on Positioning, Navigation and communication, WPNC'07, Hannover*, 2007, pp. 33-36.

[4] J. Won Kim, H.J. Jang, D. Hwang and C. Park, "A step, stride and heading determination for the pedestrian navigation system," *Journal of Global Positioning Sustems*, vol. 3 (1-2), pp.273-279, 2004.

[5] R. G. Stirling, "Development of a pedestrian navigation system using shoe mounted sensors", *Master of Science*, University of Alberta, 2003.

[6] R Stirling, J. Collin, K. Fyfe and G. Lachapelle, "An Innovative Shoe-mounted Pedestrian Navigation System", In *GNSS 2003, Graz, Austria, 22-25 April*, 2003, pp. 1-15.

[7] H. Weinberg, "Using the ADXL202 in Pedometer and Personal NavigationApplications," *Analog Devices AN-602 application Note*, 2002

[8] T.J. Brand and R.E. Phillips, "Foot-toFoot Range Measurement as an Aid to Personal Navigation,´´ in *ION 59th Annual Meeting, 23-25 June, Alburquerque, NM*, 2003, pp. 113-121.

[9] L. Ojeda and J. Borestein, "Non-GPS Navigation for Emergency Responders," In *International joint Topical Meeting on Sharing Solutions for Emergencies and Hazardous Environments, February 12-15, Salt Lake City, Utath, USA*, 2006, pp. 1-8.

[10] S. Rajagopal, "Personal dead reckoning system with shoe mounted inertial sensors," In *Master of Science Thesis, Stockholm, Sweeden*, 2008, pp. 1-45.

[11] A. Schumacher, "Integration of a GPS aided Strapdown Inertial navigatio system for land vehicles," In *Master of Science Thesis, Stockholm, Sweeden*, 2006, pp. 1-57.

[12] J. Borestein, L. Ojeda and S. Kwanmuang, "Heuristic reduction of gyro drift in IMU-based personnel tracking system," In *SPIE Defense, Security and Sensing Conference, April 13-17, Orlando, Florida, USA*, 2009, pp. 1-11.

[13] A.R. Jiménez, F. Seco, C. Prieto and J. Guevara, "A Comparison of Pedestrian Dead-Reckoning Algorithms using a Low-Cost MEMS IMU," In *6th IEEE International Symposium on Intelligent Signal Processing, 26-28 August, Budapest, Hungary*, 2009, pp. 37-42.

[14] E. Foxlin, “Pedestrian tracking with shoe-mounted inertial sensors,” *IEEE Computer graphics and Applications*, vol. 1, pp. 38-46, 2005.